An Intrinsic Velocity–Curvature–Acceleration Relationship for Weakly Unstable Gaseous Detonations

Scott I. Jackson*, Carlos Chiquete, and Mark Short

Los Alamos National Laboratory, Los Alamos, NM 87507 USA

Abstract

The shock motion of calculated weakly unstable cellular detonation was analyzed using concepts from velocity-curvature theory to develop new insight into the underlying physical mechanisms driving the cellular instability. The cellular cycle was shown to follow a surface in a three-dimensional coordinate system composed of the local shock velocity, curvature, and acceleration. Wavelets of the detonation shock were found to follow a velocity-curvature trajectory that was characteristic of an initially reactive wave that decays in time to a decoupled blast wave. Near the Mach stem, these trajectories were only modulated by the strength of the Mach stem at the time the wavelet was generated, indicating that the small reaction zone present in this region is the dominant factor driving the flow. Away from the Mach stem, all wavelet trajectories collapsed to a common curve in velocity-curvature space that was consistent with motion of a decaying blast wave. For the mixture studied, the apparent adherence of shock motion to a unique surface in velocity-curvature-acceleration space indicates the possible existence of an intrinsic mixture-specific relationship for cellular gaseous detonation. This relationship and analysis methodology also provides a mechanism for quantification of the shock velocity and shape fluctuations present in cellular detonation, which may provide utility for modeling detonation engineering applications such as rotating detonation engine design.

Keywords:
Gas-Phase Detonation, Cellular Instability

1. Introduction

Cellular instabilities are observed to occur for self-sustained detonation propagation in gaseous explosive. These instabilities arise due to the presence of acoustic-strength shock waves that propagate normal to the detonation shock surface. The presence of multiple transverse waves causes the surface of the lead shock to pulsate as alternating regions undergo different phases of the instability. In practice, a myriad of transverse wave modes are possible depending on the system geometry and explosive properties. The cellular cycle refers to the tracks traced by triple points on confining walls in the presence of multiple transverse waves, where the triple point consists of the intersection of the lead shock, Mach stem and transverse wave. Regular repeating track patterns are referred to as weakly unstable behavior, while highly irregular patterns are considered to be highly unstable detonation. Experiments have indicated that these periodic transverse wave interactions are necessary for detonation propagation [1, 2].

Recently, there has been interest in characterizing gaseous detonation propagation with velocity-curvature concepts from Detonation Shock Dynamics (DSD) theory [3–6]. DSD is a surface propagation concept that replaces the detonation shock and reaction zone with a surface that evolves according to a specified normal-velocity evolution law [7–9] and is commonly used to model condensed-phase explosives [10]. DSD assumes that the front curvature κ is small relative to the inverse of the length of the detonation reaction zone and that the front shape evolves slowly relative to the time for a particle to pass through the reaction zone. The local normal detonation velocity D_n is considered constant to leading order, with the first correction being a function of shock curvature such that $D_n = f(\kappa)$. Higher-order corrections also exist to account for the influence of time-dependent and transverse flow effects in explosives with large reaction zones [11].

*Corresponding author:
Email address: sjackson@lanl.gov (Scott I. Jackson)

Author's version of manuscript accepted to Proceedings of the Combustion Institute, Vol. 37, pp. 3601-3607, 2019.

Application of DSD to gaseous detonations introduces different complications due to the presence of the cellular instability. The impedance of most solid confiners does not allow for substantial postshock flow divergence, minimizing the magnitude of any steady wavefront curvature present in gaseous detonation confined to (cylindrical or rectangular cross-sectional) straight-channel geometries. Meanwhile, local cellular pulsations can introduce much larger local and temporal variations in D_n and κ, swamping any steady curvature and precluding determination of the D_n–κ relationship from any single experimental front shape measurement.

Nevertheless, prior work has used approximate methods to directly predict and characterize the cellular structure. Stewart et al. [12] and Yao and Stewart [13] were able to recreate this instability with a shock-evolution equation derived for weak curvature, slow temporal variations, large activation energy, and near Chapman-Jouguet (CJ) conditions. He and Calvin [14], Yao and Stewart [15] and Klein et al. [16] used numerical and approximate analytic solutions applied to gaseous detonation to predict the existence of a limiting critical κ, beyond which the detonation contained no sonic point.

Nakayama et al. [3] established a D_n–κ relationship for ethylene-oxygen mixtures. They addressed the above complications by propagating the detonation around a curved channel, which induced significant quasi-steady wavefront curvature in excess of that created by the cellular instability. Their imaging technique also smoothed the wavefront shape by integrating over multiple cell cycles. Instability effects were also mitigated by working with sufficiently sensitive mixtures to allow an excess of 32 cells across the channel. This work described a global and nondimensional D_n–κ relation for the mixtures tested [3, 4].

Recent work by Borzou and Radulescu [6] similarly induced curvature on the detonation wavefront with a specially shaped diverging channel intended to generate a globally constant flow divergence. Their results also inferred a mean D_n–κ relationship for the weakly and highly unstable mixtures studied by effectively averaging over the effects of the cellular instability. Such approaches highlight DSD's intended goal of accurately predicting wave shape and timing while neglecting the smaller-scale details of the wave structure. These approaches show promise for predicting detonation wave timing and shape in engine technologies, where accurate wave arrival predictions and efficient simplified modeling strategies can be used to improve optimization of rotating detonation engine system performance [17–19].

For application, however, it is also critical to estimate the magnitude of the wave timing variations that can result from the cellular fluctuations. In addition to providing utility in approximating detonation front timing and wave shape for engineering applications, analyzing the velocity-curvature characteristics of detonation can also provide substantial insight into the underlying cellular instability physics, including the degree of shock-reaction coupling and the sensitivity of the detonation to flow divergence. For example, ideal (or very sensitive), insensitive, and nonideal detonation in high explosives all exhibit characteristically different trends in D_n–κ space, as discussed in Refs. 5 and 10. Increasingly nonideal detonations have spatially larger reaction zones and are seen to have a greater dependence of detonation velocity on wave curvature, support detonation over a more limited curvature span, and thus are more influenced by wave geometry and confinement. It is possible that such analysis could also be used to explain the fundamentally different mechanisms driving cellular instabilities in weakly unstable and highly irregular detonation. Despite this, relatively little work has been performed on this topic. An exploratory work by Jackson and Short [5] experimentally and computationally measured the D_n–κ relationship in the detonation cell for weakly unstable mixtures and found that the resulting profiles were heavily influenced by the unsteady nature of the cellular cycle. Rather than forming a unique profile in D_n–κ space, different portions of the cellular detonation front were observed to correspond to both highly reactive detonation waves and diffracting inert blast waves at any given time. Thus, analysis of each shock shape image required signifiant interpretative analysis.

In this study, we extend the prior work of Jackson and Short [5] to quantitatively explore the influence of the flow unsteadiness. Rather than analyzing the D_n–κ profiles of the full shock front at each instant of the wave motion, as is commonly done for quasi-steady shocks, we instead follow the D_n–κ path traced in time by infinitesimally small segments of the shock throughout the cellular cycle. This approach is more intuitive and clearly confirms prior interpretations of the detonation dynamics present in these weakly unstable flows. More significantly, *we show conclusively that the cellular cycle follows a unique surface in velocity-curvature-acceleration space.* We anticipate that this discovery will enable a new methodology for simplifying and studying the complex wave dynamics generated by the cellular instability.

2. Numerical Simulation Details

We use high-resolution numerical simulation to analyze the dynamics of normal detonation velocity (D_n), acceleration ($\dot{D}_n = \frac{\mathrm{D}}{\mathrm{D}t}(D_n)$), and curvature ($\kappa$) variation in weakly unstable detonation cells. Prior work has shown that this approach is consistent with experimental results, which are limited in spatial and temporal resolution [5]. For consistency, we choose to use similar methodology and mixture parameters to the computational component of our prior work [5] but a higher axial resolution.

The non-dimensional reactive Euler equation model for an ideal gas was used for the simulations with a one-step Arrhenius-type reaction rate. The flow and progress equations are

$$\begin{aligned} \frac{D\rho}{Dt} + \rho(\nabla\cdot\mathbf{u}) = 0, \quad \frac{D\mathbf{u}}{Dt} = -\frac{1}{\rho}\nabla p, \\ \frac{De}{Dt} = -\frac{p}{\rho}(\nabla\cdot\mathbf{u}), \quad \frac{D\chi}{Dt} = W, \end{aligned} \tag{1}$$

with density ρ, specific internal energy e, velocity $\mathbf{u} = (u, v)$, and reaction progress variable χ. Reference values for the original dimensional variables are the initial reactant density $\tilde{\rho}_0$, initial reactant pressure $\tilde{p}_0$, $\sqrt{\tilde{p}_0/\tilde{\rho}_0}$ (velocity) and $\tilde{p}_0/\tilde{\rho}_0$ (specific internal energy), where the tilde $\{\tilde{}\}$ denotes a dimensional quantity. Parameter $D_n = \tilde{D}_n/\sqrt{\tilde{p}_0/\tilde{\rho}_0}$ and the equation of state for an ideal gas is used

$$e = \frac{p}{\rho(\gamma-1)} - Q\chi, \quad T = p/\rho, \tag{2}$$

where γ is the ratio of specific heats and T is the temperature, which is normalized by the initial reactant temperature $\tilde{T}_0$. The reaction rate W is

$$W = k(1-\chi)\exp(-E\rho/p). \tag{3}$$

We study a mixture with $E = \tilde{E}/\tilde{R}\tilde{T}_0 = 20$, $Q = \tilde{Q}/\tilde{R}\tilde{T}_0 = 10$ and $\gamma = 1.54$, where $\tilde{R}$ is the specific gas constant, Q is the heat release, and E is the activation energy. Time is scaled with $\tilde{l}_{1/2}/\sqrt{\tilde{p}_0/\tilde{\rho}_0}$. The reaction length is also scaled with $\tilde{l}_{1/2}$, the distance between the shock and the point where half the reaction is completed. The non-dimensional rate constant $k = 22.719$. Dimensional reference values are given in Table 1. Parameters E, Q, and γ approximate the calculated one-dimensional Zeldovich-Von Neumann-Döring (ZND) Mach number, post-shock γ, and postshock ignition delay sensitivity in constant volume ignition simulations at the post-shock state using calculated detonation states from the $2H_2$–O_2–Ar kinetic mechanism of Ref. [20]. Dimensional values and the resulting calculated instability behavior were previously [5] determined to be consistent with the initial conditions of the $2H_2$+O_2+80%Ar detonation cell experiment described in Ref. [21].

$\tilde{p}_0$	0.2 bar
$\tilde{\rho}_0$	0.2778 kg/m^3
$\sqrt{\tilde{p}_0/\tilde{\rho}_0}$	268.3 m/s
$\tilde{T}_0$	298 K
$\tilde{D}_{CJ}$	1480.2 m/s
$\tilde{l}_{1/2}$	0.72 mm
$\tilde{l}_{1/2}/\sqrt{\tilde{p}_0/\tilde{\rho}_0}$	2.68μs

Table 1: Dimensional reference values for the numerical simulation. Here $\tilde{l}_{1/2}$ is the distance between the ZND shock and the point where half the reaction is complete.

The solution method uses the two-dimensional shock-fit shock-attached algorithm and code described in Chiquete et al. [22, 23]. The algorithm uses a Lax-Friedrichs flux splitting spatial discretization and temporal integration via a second-order two-stage Heun's method. The shock-attached system allows straightforward determination of the lead shock curvature (using the calculated detonation shock slope) and normal detonation velocity. The two-dimensional shock-fit, shock-attached methodology has previously been used to explore the linear stability and nonlinear dynamics of detonation cell development for the ideal condensed-phase detonation model [24].

The calculated two-dimensional channel has rigid wall flow conditions at the transverse walls, a width of 9 (dimensionally 9 times $\tilde{l}_{1/2}$) and a computational zone length of 50. The lead shock is fixed at $z = 0$ with an outflow boundary at $z = -50$. The resolution is 0.025 both axially and transversely, yielding 40 points per $\tilde{l}_{1/2}$. The resolution sensitivity for cellular detonations computed with the two-dimensional shock-fit shock-attached algorithm [25, 26] is discussed in Short et al. [24] and limits the channel width to the listed values. A one-dimensional ZND structure was initially imposed across the channel containing a spatial perturbation in the initial shock front position to generate the cellular instability.

3. Results

Figure 1 shows the pressure distribution in the channel for a calculated timestep. The cellular structure is evident with development of a single cell in the channel

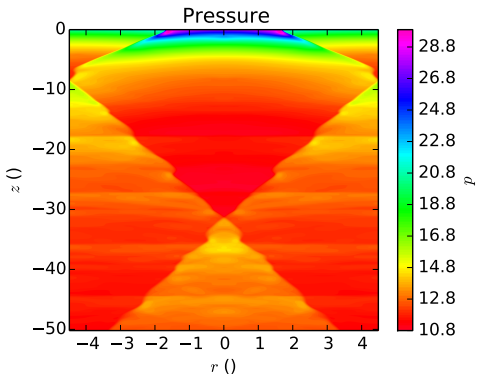

Figure 1: Snapshot of the calculated pressure distribution for a cellular instability in the weakly unstable mixture. Values are nondimensional. Color scale denotes pressure.

as indicated the presence and path of the two reflected shocks. Figure 2 shows the evolution of D_n from the initial ZND wave along the channel centerline with time. Small oscillations in D_n around $D_{CJ} = 5.517$ grow to a weakly unstable and near periodic limit cycle corresponding to fully nonlinear cellular detonation.

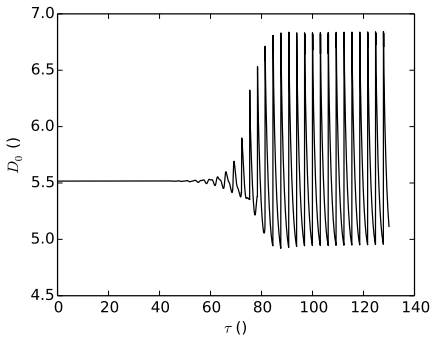

Figure 2: D_n vs. time along the channel centerline indicating the onset of weakly unstable cellular detonation.

Figure 3 shows instantaneous shapes of the shock loci in black over one detonation cell duration for the last cycle shown in Fig. 2 and illustrates that a single cell develops for the channel width of 9. The colored lines overlaid on the shock loci approximate the paths of infinitesimally thin segments of the detonation shock wave, which we refer to as wavelets, across the cellular evolution. These paths are started at specified initial starting points on the shock front, which are the cell edges for each timestep shown. They are then evolved by successively extending a line segment from the shock normal in the present timestep to the intersection of the

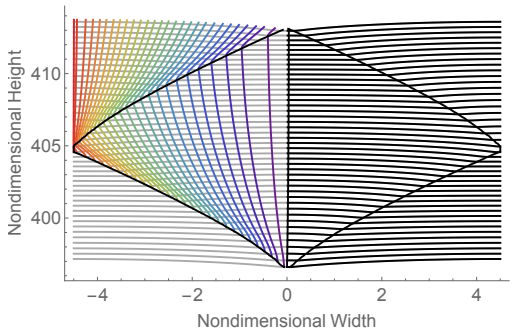

Figure 3: Shock loci for successive timesteps (black curves) and wavelet paths (colored curves). The wavelet color (blue-to-red) indicates increasing initial distance from the cell centerline.

shock front in the following timestep. The wavelets are seen to initially turn steeply away from the cell centerline shortly after their initiation near the triple point before gradually turning back towards the centerline later in their cycle.

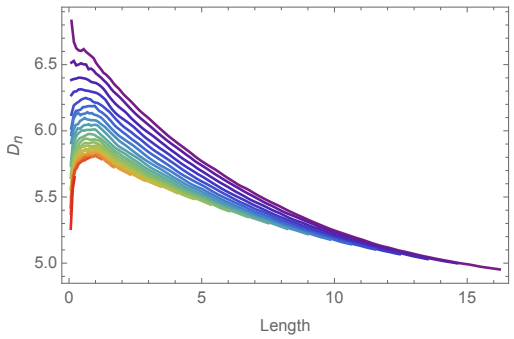

Figure 4: Evolution of local normal shock speed D_n versus distance for each wavelet path and color scale in Fig. 3.

The local shock speed D_n of the wavelets versus distance are plotted in Fig. 4 with distance shifted such that the origin denotes the wavelet initiation point at the growing cell edge. Each curve ends when the wavelet encounters the triple point terminating the cell. The resulting series of curves are seen to neatly nest together and exhibit similar behavior. For each curve, the shock velocity increases dramatically as the wavelet is generated. The shock velocity then peaks very close to generation point (near a nondimensionalized length of 0.75). Following that peak, the wavelet velocity smoothly decays with increasing distance until it encounters the cell end. The peak D_n value is seen to decrease for successive paths, indicating a weakening of the Mach stem source with distance from the cell center.

Figure 5 plots the local curvature for each wavelet versus distance travelled after initiation. The curvatures

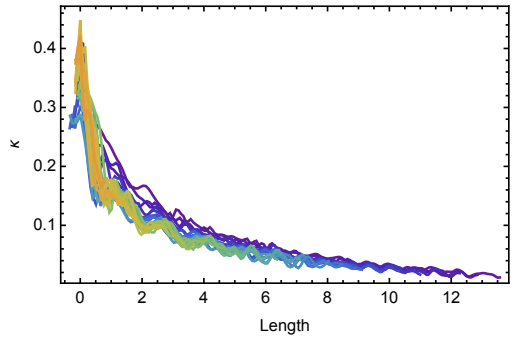

Figure 5: Evolution of local curvature κ in length for each wavelet path and color scale in Fig. 3.

are seen to decrease rapidly with length and are seen to not vary significantly with path. This would also imply that the shock curvature is not a dominant factor in the reaction dynamics for this mixture (though we see this is not always the case for other mixtures not discussed here). Additionally, the wavelets are seen to spend very little length (and time) of the cell cycle in the high curvature (κ = 0.1–0.4 regime). The trajectories also display small high-frequency oscillations that are a result of the curvature calculation performed in post-processing, which involves interpolation of the second derivative of the shock shape.

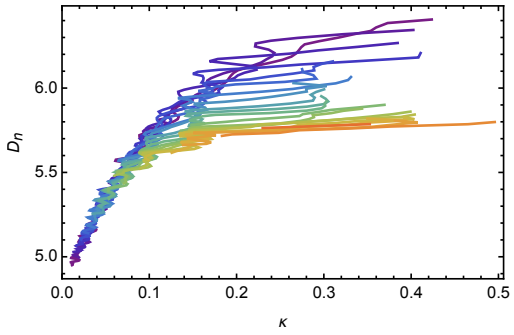

Figure 6: The velocity–curvature (D_n–κ) trajectories of each wavelet and color scale in Fig. 3.

Parametrically plotting D_n versus κ in Fig. 6 shows the trajectory of each path in velocity–curvature space. Each wavelet trajectory is seen to follow a similar profile, starting at a high D_n and κ before decreasing as the wavelet decays. The decaying trajectories eventually overlay in D_n–κ space.

Previously, Jackson and Short [5] plotted profiles in D_n–κ space from successive shock loci. Their analysis showed that each shock locus contained three possible velocity–curvature regimes: (1) a small slope, large-curvature-span curve characteristic of a spatially small reaction zone, (2) a high-slope, narrow-curvature-span line consistent with a nonreactive, decaying cylindrical blast wave, (3) a transitional region between these two limiting behaviors. Growing cells were shown to contain all three regimes, with features 1 and 2 predominant in young growing cells. Decaying cells contained only regime 3. Thus, regimes 1 and 2 were associated with the presence of a reactive Mach stem. In the present study, it can be seen that all wavelets initiated by the Mach stem follow a similar trajectory in regime 1 that is only modulated by the value of D_n or the strength of the Mach stem at the time of wavelet initiation. As the wavelets move away from the reactive Mach stem, they very quickly assume a common decaying cylindrical profile.

The significant unsteadiness present in the cellular instability clearly modulates the early behavior of each wavelet studied. Thus, it is desirable to explore if the wave motion is a function of the level of unsteadiness. We represent the amount of wave unsteadiness by local acceleration or the Lagrangian derivative of the normal shock velocity $\frac{\mathrm{D}}{\mathrm{D}t}(D_n) = \dot{D}_n$ following a fluid element. The unsteady wave behavior has been seen to evolve across a D_n–κ–$\dot{D}_n$ surface in prior work by Yao and Stewart [13] for stable condensed-phase explosive parameters. Figure 7 plots values of $\dot{D}_n$ versus D_n as

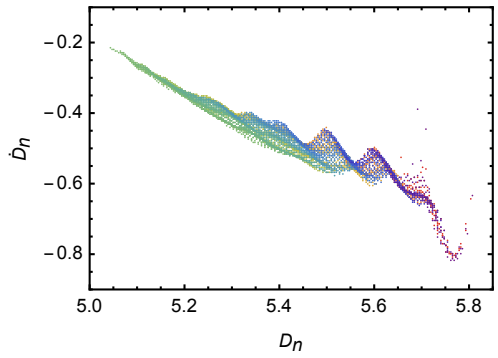

Figure 7: Evolution $\dot{D}_n$ versus D_n for each wavelet path shown in Fig. 3 for each wavelet path and color scale in Fig. 3. Data is shown as points, rather than curves, to better visualize the overlay of the trends for different wavelets.

computed from the derivative of spline fits to the present D_n–t data. The $\dot{D}_n$ data is seen to be restricted to a near linear trend in $\dot{D}_n$–D_n space that evolves weakly with the wavelet location in the cell. Only data at high D_n values (near the edge of the growing cell, which is a high gradient region [5]) deviates from this trend by moving sharply off the top of the vertical scale in Fig. 7.

The combined trend of the cellular instability in D_n–

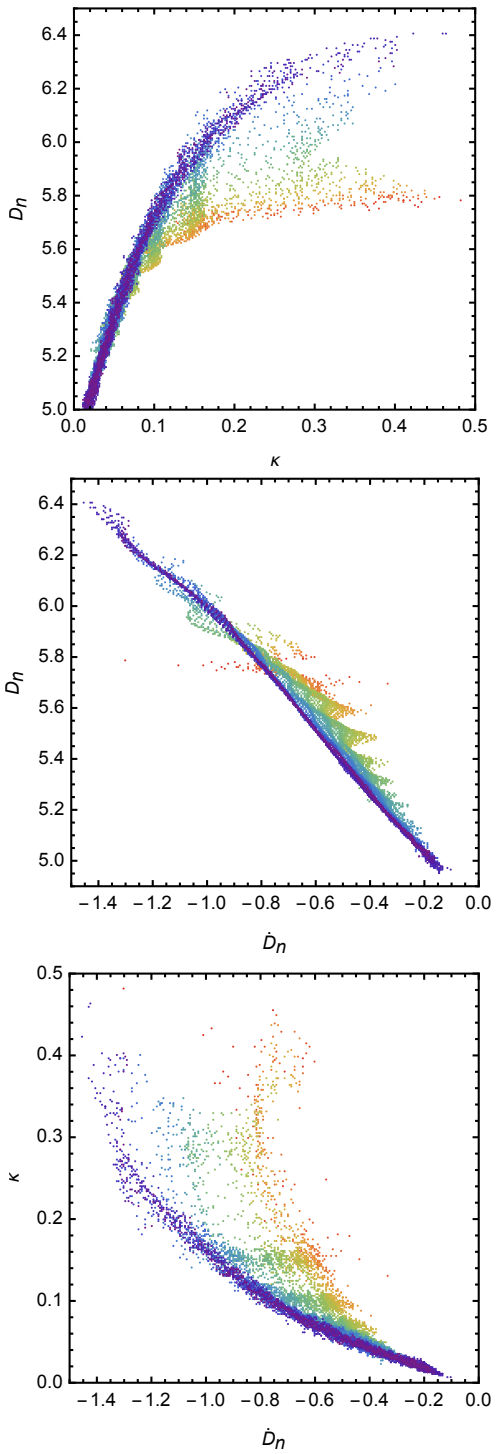

Figure 8: D_n–κ plane (top), D_n–$\dot{D}_n$ plane (middle), and $\dot{D}_n$–κ plane (bottom) for each wavelet path and color scale in Fig. 3.

κ–$\dot{D}_n$-space is shown in Figs. 8–9. Figure 8 plots the projections of the three-dimensional behavior onto the D_n–κ plane (top), D_n–$\dot{D}_n$ plane (middle), and $\dot{D}_n$–κ plane (bottom). Perspective views are shown in Fig. 9 to aid in visualization of the three-dimensional structure. The data is seen to form a surface, which captures the previously discussed trends. At higher velocities and curvatures, the span of the surface is large in the D_n and κ directions. At lower velocities and curvatures, the span contracts dramatically in D_n and less dramatically in the κ direction. In the D_n–$\dot{D}_n$ plane, the data is seen to remain roughly confined to an almost linear curve.

The adherence of this weakly unstable flow a D_n–κ–$\dot{D}_n$ surface provides substantial future opportunity. Firstly, the observed relationship quantifies the range and magnitude of these physical parameter variations (D_n, κ, and $\dot{D}_n$) present in the wave for the first time. Previously this relationship has only been explored for centerline cell velocities [27]. These quantified variations could be used in addition to the quasi-steady theories [3, 4, 6] to predict the uncertainties in wave arrival times and shape.

Secondly, it is possible that this relationship could be used to compute cellular detonation in analogous fashion to condensed-phase flows with a proper edge angle [8] treatment at the cell boundary (an issue that remains unexplored at present). Such an approach would be more involved than leading-order DSD theories, but possibly be similar in complexity to DSD approaches for more non-ideal flows [28].

Finally, studying the variations of this D_n–κ–$\dot{D}_n$ relationship across a broad range of mixture stability is expected to yield insight into the mechanisms driving cellular instability. For example, it is now clear from the weakly unstable case studied that the wave is only coupled and reactive very close to the start of the cell and follows a self-consistent decaying profile after decoupling. Variations in the duration of these reactive and decaying regimes are expected with varying mixture stability.

4. Conclusions

High-resolution calculations have been performed of weakly unstable detonation. The perturbations of the cellular instability on the shock front were analyzed in velocity-curvature space by following the local normal shock velocity D_n and curvature κ evolution of shock front portions or wavelets in time. Wavelets were found to follow a similar trajectory in velocity-curvature space that was characteristic of an initially reactive wave that decayed in time to a decoupled blast wave. Near the Mach stem, these trajectories were only modulated by the strength of the Mach stem at the time the wavelet

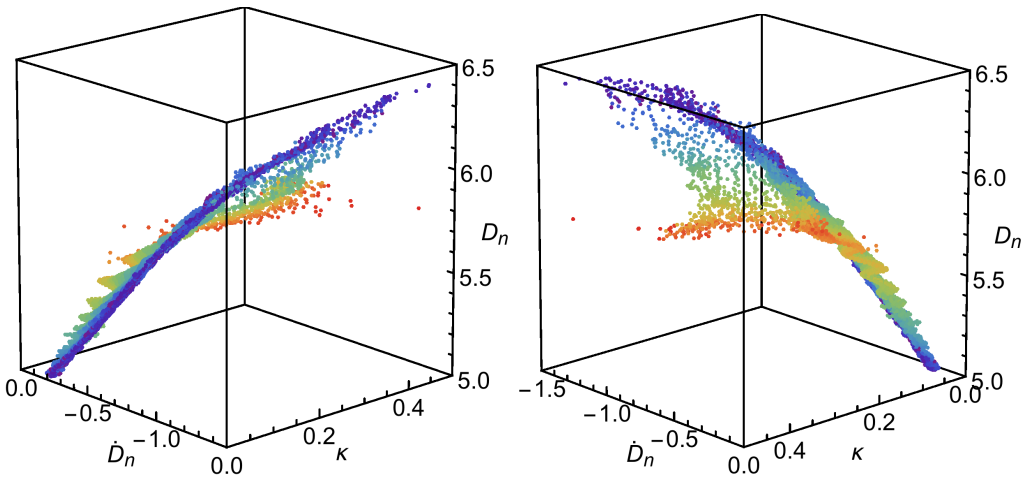

Figure 9: Three-dimensional perspective views of the D_n–κ–$\dot{D}_n$ surface traced by the cellular instability for each wavelet path and color scale in Fig. 3. The two views differ by a 180° rotation around the (vertical) D_n axis.

was generated, indicating that the small reaction zone present in this region is the dominant factor driving the flow. Away from the Mach stem, all wavelet trajectories collapsed to a common curve in velocity-curvature space that was consistent with motion of a decaying blast wave. The unsteadiness of the shock front was also quantified via the derivative of the local shock velocity in time ($\dot{D}_n$) and the cellular instability data was shown to correlate with this parameter by forming a surface in D_n–κ–$\dot{D}_n$-space. It is expected that studying the variation of the cellular instability in D_n–κ–$\dot{D}_n$-space for mixtures of increasing instability may yield new insight into the underlying physical mechanisms driving this instability through clarification of any dominant dynamics present in these complex systems.

References

[1] J. Lee, The Detonation Phenomenon, Cambridge University Press, New York, 2008.

[2] M. Radulescu, J. Lee, Combustion and Flame 131 (2003) 29–46.

[3] H. Nakayama, T. Moriya, J. Kasahara, A. Matsuo, Y. Sasamoto, I. Funaki, Combustion and Flame 159 (2012) 859–869.

[4] H. Nakayama, J. Kasahara, A. Matsuo, I. Funaki, Proceedings of the Combustion Institute 34 (2013) 1939–1947.

[5] S. I. Jackson, M. Short, Combustion and Flame 160 (2013) 2260–2274.

[6] B. Borzou, M. I. Radulescu, arXiv preprint arXiv:1606.05323 (2016).

[7] J. Bdzil, Journal of Fluid Mechanics 108 (1981) 195–226.

[8] J. B. Bdzil, W. Fickett, D. S. Stewart, Ninth Symposium (Int.) on Detonation (1989) 730–742.

[9] J. Bdzil, D. Stewart, Ann. Rev. Fluid Mech. 39 (2007) 263–292.

[10] S. I. Jackson, M. Short, Journal of Fluid Mechanics 773 (2015) 224–266.

[11] J. Bdzil, T. Aslam, M. Short, Twelfth Symposium (Int.) on Detonation (2002) 409–417.

[12] D. Stewart, T. Aslam, J. Yao, in: Proceedings of the 26th International Symposium on Combustion, volume 26, Combustion Institute, Pittsburgh, PA, 1996, pp. 2981–2989.

[13] J. Yao, D. S. Stewart, Journal of Fluid Mechanics 309 (1996) 225–275.

[14] L. He, P. Calvin, Journal of Fluid Mechanics 277 (1994) 227–248.

[15] J. Yao, D. Stewart, Combustion and Flame 100 (1995) 519–528.

[16] R. Klein, J. Krok, J. Shepherd, Curved Quasi-Steady Detonations: Asymptotic Analysis and Detailed Chemical Kinetics, Technical Report FM95-04, Graduate Aeronautical Laboratories, California Institute of Technology, Pasadena, CA, 1996.

[17] F. K. Lu, E. M. Braun, Journal of Propulsion and Power (2014) 1125–1142.

[18] B. A. Rankin, D. R. Richardson, A. W. Caswell, A. G. Naples, J. L. Hoke, F. R. Schauer, Combustion and Flame 176 (2017) 12–22.

[19] J. E. Shepherd, J. Kasahara, Analytical Models for the Thrust of a Rotating Detonation Engine, Technical Report GALCIT Report FM2017.001, California Institute of Technology, 2017.

[20] J. Li, Z. Zhao, A. Kazakov, F. L. Dryer, Int. J. Chem. Kinet. 36 (2004) 566–574.

[21] J. Austin, The Role of Instability in Gaseous Detonation, Ph.D. thesis, California Institute of Technology, 2003.

[22] C. Chiquete, M. Short, C. D. Meyer, J. J. Quirk, Combustion Theory and Modelling (2018) 1–33.

[23] C. Chiquete, M. Short, C. Meyer, J. Quirk, in: 2017 International Colloquium on the Dynamics of Explosions and Reactive Systems (ICDERS), p. 1077.

[24] M. Short, I. Anguelova, T. Aslam, J. Bdzil, A. Henrick, G. Sharpe, Fluid Mechanics 595 (2008) 1–21.

[25] A. Henrick, T. Aslam, J. Powers, J. Computat. Phys. 213 (2006) 311–329.

[26] A. Henrick, Shock-fitted numerical solutions of one- and two-dimensional detonation, Ph.D. thesis, University of Notre Dame, 2008.

[27] R. Strehlow, A. Crooker, Acta Astronautica 1 (1974) 303–315.

[28] J. Bdzil, M. Short, G. Sharpe, T. Aslam, J. Quirk, in: 13th Symposium (Int.) on Detonation, Office of Naval Research, 2006, pp. 726–736.